A Novel Powder Metallurgy Processing Approach to Prepare Fine-Grained Cu-Al-Ni Shape-Memory Alloy Strips from Elemental Powders

S.K. VAJPAI, R.K. DUBE, P. CHATTERJEE, and S. SANGAL

The current work describes the experimental results related to the successful preparation of fine-grained, Cu-Al-Ni, high-temperature shape-memory alloy (SMA) strips from elemental Cu, Al, and Ni powders via a novel powder metallurgy (P/M) processing approach. This route consists of short time period ball milling of elemental powder mixture, preform preparation from milled powder, sintering of preforms, hot-densification rolling of unsheathed sintered powder preforms under protective atmosphere, and postconsolidation homogenization treatment of the hot-rolled strips. It has been shown that it is possible to prepare chemically homogeneous Cu-Al-Ni SMA strips consisting of equiaxed grains of average size approximately 6 μm via the current processing approach. It also has been shown that fine-grained microstructure in the finished Cu-Al-Ni SMA strips resulted from the pinning effect of nanosized alumina particles present on the grain boundaries. The finished SMA strips were almost fully martensitic in nature, consisting of a mixture of β_1'- and γ_1'-type martensites. The Cu-Al-Ni SMA strips had 677 MPa average fracture strength, coupled with 13 pct average fracture strain. The fractured surfaces of the specimens exhibited primarily dimpled ductile type of fracture, together with some transgranular mode of fracture. The Cu-Al-Ni strips exhibited an almost 100 pct one-way shape recovery after bending followed by unconstrained heating at 1, 2, and 4 pct applied deformation prestrain. The two-way shape-memory strain was found approximately 0.35 pct after 15 training cycles at 4 pct applied training prestrain.

DOI: 10.1007/s11661-012-1081-0

I. INTRODUCTION

SHAPE-memory alloys (SMAs) have received a considerable amount of attention in recent decades because of their viability of potential applications in a variety of areas including automotive, aerospace, and biomedical applications.[1–5] As a result, several types of SMAs, such as Ni-Ti-based, Cu-based, and Fe-based alloys, have been developed according to specific requirements.[1–6] Among these SMAs, Cu-based shape-memory alloys have been considered a potential material for applications such as high-damping capacity material, sensors, and actuators. In particular, Cu-Al-Ni alloys have been found suitable for high-temperature applications because of their high thermal stability at increased temperatures, *i.e.,* above 373 K (100 °C).[4–8] However, the Cu-Al-Ni alloys prepared by conventional casting method suffered with the problem of severe brittleness as a result of large grain sizes (up to several millimeters) coupled with large elastic anisotropy.[6,9,10] Hence, several attempts were made to enhance the ductility of conventionally cast Cu-Al-Ni alloys through grain refining by addition of a fourth element, such as Ti, Zr, Mn, B, Y, V, and rare earths.[11–19] The grain size of the resulting Cu-Al-Ni alloys was found to lie in the range of 100 to 800 μm. The grain refinement via alloying additions exhibited improvement in the mechanical properties of the Cu-Al-Ni alloys. However, the mechanical properties of these alloys were still unsatisfactory for most practical applications.

A few attempts have been made to prepare fine-grained Cu-Al-Ni alloys, with a grain size less than 100 μm, via different powder metallurgy routes. These routes were based on the Cu-Al-Ni alloy powder that was prepared by either inert gas atomization process or mechanical alloying of elemental powders in a high-energy ball mill under inert gas atmosphere. The consolidation of these powders was carried out by sintering, hot pressing, hot isostatic pressing, hot extrusion, hot swaging, hot-densification rolling, or a combination of these. One important feature of the Cu-Al-Ni SMAs produced by powder metallurgy routes was that the products had a fine grain size vis-à-vis those produced from the liquid metallurgy route. As a result, near full-density powder metallurgy Cu-Al-Ni SMAs exhibited superior mechanical properties.

There have been some attempts to prepare fine-grained Cu-Al-Ni alloys starting with inert gas atomized prealloyed powders.[20–25] It was found that the Cu-Al-Ni SMA prepared from inert gas atomized powders exhibited superior mechanical properties compared with

S.K. VAJPAI, Research Scholar, R.K. DUBE and S. SANGAL, Professors, and P. CHATTERJEE, Graduate Student, are with the Department of Materials Science and Engineering, Indian Institute of Technology Kanpur, Kanpur, Uttar Pradesh 208016, India. Contact e-mail: vajpaisk@iitk.ac.in

Manuscript submitted September 13, 2011.
Article published online February 10, 2012

conventionally cast material. However, only a few efforts have been made to prepare Cu-Al-Ni SMA starting with elemental powders. Tang *et al.*[26] prepared Cu-Al-Ni alloy powders from elemental powders via mechanical alloying (MA) under inert atmosphere in a high-energy ball mill after milling for 20 to 40 hours. Subsequently, the mechanically alloyed Cu-Al-Ni alloy powder was cold compacted and sintered at 1223 K (950 °C) for 20 hours under an argon atmosphere. As expected, the sintered compacts had relatively large amounts of total porosity, which led to poor mechanical and shape-memory properties. Li *et al.*[27] consolidated mechanical alloyed Cu-Al-Ni-Mn powder, prepared by high-energy ball milling under inert atmosphere, by vacuum hot pressing at 30 MPa and 1123 K (850 °C). Subsequently, the hot-pressed compacts, with a relative density of approximately 94 pct, were canned in copper capsules, and the capsules were evacuated for the removal of air. The canned and evacuated capsules were hot extruded at 1173 K (900 °C) using extrusion ratio of 90:1. The authors observed no residual porosity in the extruded material and reported 100 pct shape-memory recovery for 100 bending-heating-cooling cycles at 4 pct applied prestrain. However, no details of the mechanical properties of the materials were reported. It is apparent that the requirements of long milling time, inert milling atmosphere, and encapsulation of milled powder preforms during hot extrusion made this processing route complex and expensive. Furthermore, little work has been carried out using this powder metallurgy processing approach, and comprehensive information is lacking regarding microstructural characteristics, shape memory, and mechanical properties of alloys produced via this approach.

It is envisaged that the powder metallurgy route to prepare fine-grained Cu-Al-Ni SMA could become economically more attractive if the route is based on elemental Cu, Al, and Ni powders and the alloying is brought about during sintering of the preforms prepared from elemental powders. Recently, Sharma *et al.*[28,29] proposed and developed such a route for preparing the Cu-Al-Ni SMA strip. The route consisted of mechanical blending of elemental powders in the required proportion, cold compaction, sintering, and hot-densification rolling of unsheathed/uncanned sintered powder preforms followed by postdensification homogenization of hot-rolled strips. This processing approach was simple and reduced considerably the complexities associated with the preparation of Cu-Al-Ni SMA starting from either argon atomized or mechanically alloyed powders. The finished hot-rolled Cu-Al-Ni strips had a fracture stress of 476 MPa coupled with approximately 5 pct fracture strain. The shape-memory tests showed almost 100 pct shape recovery after 10 thermomechanical cycles in the hot-rolled strips at 1 and 2 pct applied prestrain. However, the one-way shape recovery deteriorated beyond 2 pct applied prestrain. One main reason for the low fracture strain value is that the air-atomized Al powder was used, which resulted in higher amounts of alumina (Al_2O_3) on the grain/particle boundaries leading to hindrance in full densification of the strip during hot rolling.[28] Furthermore, it is not unlikely that some Cu, Al, and Ni-rich second-phase particles were formed during sintering of the compacts prepared from a mechanically blended elemental powder mixture.[29] This could also have affected the mechanical properties.

In the current work, a novel powder metallurgy processing approach has been proposed for preparing a fine-grained Cu-Al-Ni SMA strip starting with elemental powders. The proposed route uses argon-atomized aluminum powder, instead of an air-atomized one, to minimize the residual Al_2O_3 particles in the finished strip. Furthermore, elemental powders are milled mechanically in a high-energy ball mill for a short period of time using acetone as the medium. It is envisaged that the ball milling would result in uniform distribution of Al and Ni in Cu. Recently, Vajpai *et al.*[30] showed that the wet ball milling of the mixture of Cu, Al, and Ni powder for 8 hours in acetone gives a lamellar structure in which fine layers of Cu and Al form. Such a microstructure of the ball-milled powders is expected to result in better chemical homogeneity in the sintered preforms. It is also envisaged that milling would lead to a uniform distribution of alumina particles, which might be present in small amounts on the surface of the argon-atomized aluminum powder. As a result, any possibility of segregation of alumina particles would also be minimized.

The proposed powder metallurgy route for preparing Cu-Al-Ni shape-memory alloy strip consists of wet ball milling of the elemental Cu, Al, and Ni powders in the required proportions in a high-energy ball mill for a short period of time using acetone as a process control agent. Subsequently, powder preforms are prepared from the milled powder. On a laboratory scale, powder preforms can be prepared by cold die compaction. The powder preforms are sintered at 823 K (550 °C) in hydrogen atmosphere. The sintered preforms, in unsheathed/uncanned condition, are hot rolled at 1273 K (1000 °C) under a protective atmosphere. The hot-rolled strips are then homogenized at 1223 K (950 °C) to achieve chemical homogeneity in the strip.

An attempt has been made to develop the preceding proposed route for making Cu-Al-Ni SMA strips on a laboratory scale. This article describes the experimental results related to the successful preparation of near-full density fine-grained Cu-Al-Ni shape-memory alloy strips by the proposed powder metallurgy route. The microstructural evolution at every stage of processing has been presented and discussed. The microstructural characteristics and the mechanical and shape-memory properties of the finished Cu-Al-Ni alloy strips have also been evaluated and discussed.

II. EXPERIMENTAL PROCEDURE

In the current work, elemental Cu powder (median particle size = 38.0 μm, >99 pct pure), argon atomized Al powder (median particle size = 15.0 μm, >99 pct pure), and Ni powder (median particle size = 9.0 μm, >99 pct pure) were used as a starting material. Figure 1 shows the morphology of the starting elemental Cu, Al, and Ni powders. Elemental Cu and Ni powders were

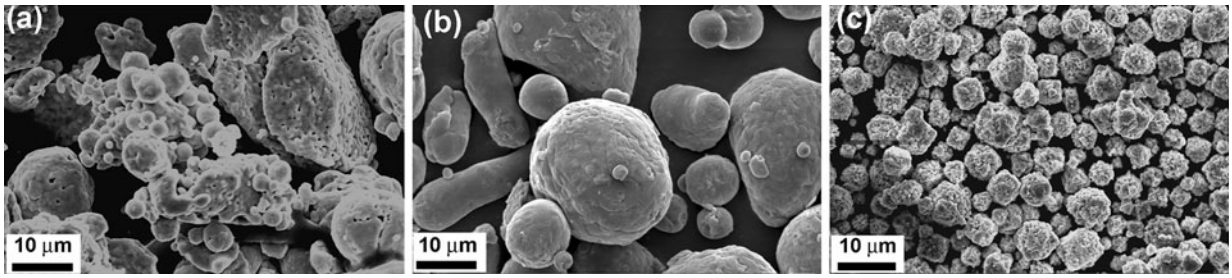

Fig. 1—SEM micrographs showing morphology of starting (*a*) Cu, (*b*) Al, and (*c*) Ni powder.

annealed in H_2 atmosphere at 773 K (500 °C) for 30 minutes for reducing the surface oxides on the powders. The objective of the current work is to prepare martensitic Cu-Al-Ni alloy strips, *i.e.,* aluminum content in the Cu-Al-Ni alloy must lie in the range of 11 to 14 wt pct. It is possible that some aluminum may be consumed in forming alumina particles during ball milling. Moreover, the possibility of formation of some intermetallics, containing aluminum, during the processing of Cu-Al-Ni strips cannot be ruled out. These factors might reduce the amount of aluminum in the final Cu-Al-Ni alloy strips. Therefore, it was decided to start with a 14 wt pct Al in the starting powder mixture. The elemental Cu, Al, and Ni powder mixture with a composition of 82Cu–14Al–4Ni (wt pct), was milled in Fritsch Pulverisette 5 high-energy planetary ball mill (Fritsch, Idar-Oberstein, Germany) rotating at 300 rpm for various time periods to optimize the desired milling time. The ball milling was carried out using high Ni-Cr steel vials, high Ni-Cr balls as grinding media, and acetone as a process control agent. The ball-to-powder ratio of 8:1 was maintained for each run.

The milled powders were cold compacted in a rectangular die at 500 MPa pressure to prepare "green" compacts/preforms. The cold-compacted rectangular preforms had dimensions 30 mm (L) × 18 mm (W) × 6 mm (T), and its green density was approximately 75 pct of the calculated theoretical. The green preforms were sintered at 823 K (550 °C) for 1 h in a hydrogen atmosphere. Subsequently, the sintered preforms were hot rolled at 1273 K (1000 °C), and near-full density strips were prepared after approximately 85 pct thickness reduction. The hot rolling was carried out in a specially designed rolling mill system in which the reheating furnace was interlinked with the hot-rolling mill, and the sintered preforms remained under the hydrogen atmosphere right up to the nip of the rolling mill to avoid any oxidation of the sintered powder preforms during hot rolling. The specimens were annealed for 15 minutes at 1273 K (1000 °C) between two consecutive hot-rolling passes. The hot-rolled strips were placed in a bed of graphite immediately to avoid any oxidation of hot-rolled strips not only on the surface but also inside the porous strips. A two-high rolling mill, with a roll diameter 127 mm and rotating at 80 rpm, was used for hot rolling. The rolls were not heated prior to hot rolling. The hot-rolled strips were homogenized under inert gas atmosphere (Argon) at 1223 K (950 °C) for 6 hours to achieve proper chemical homogeneity.

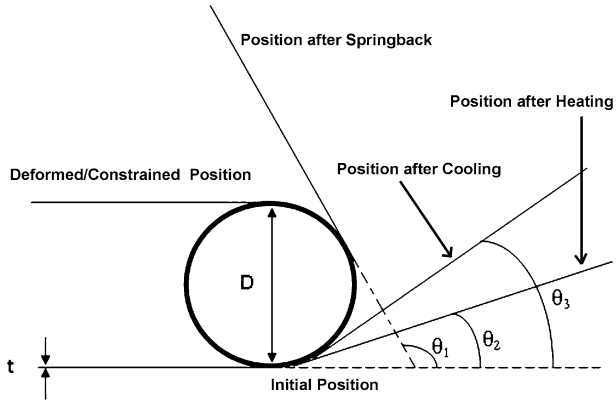

Fig. 2—A schematic diagram of the bend test arrangement.

The strips were quenched in water at room temperature after the homogenization.

The phase evolution in the Cu-Al-Ni SMA strips was studied by X-ray diffraction (XRD) technique using monochromatic Cr Kα (0.228970 nm) radiation. The microstructural characterization and elemental compositional analysis was carried out by scanning electron microscopy and energy dispersive spectroscopy (EDS). The transformation temperatures of heat-treated Cu-Al-Ni alloy strips were evaluated by performing calorimetric studies at a heating–cooling rate of 20 K/min (20 °C/min.). The mechanical properties of the Cu-Al-Ni strips were evaluated by performing a tension test on the specimen in martensitic state. The subsize specimens with 25-mm gauge length were prepared from the strips according to ASTM E8/E8M specifications. The thickness of the specimen was maintained at approximately 0.6 mm for all the specimens. The tension tests were carried out on a Lloyd EZ machine at a strain rate of 6.67×10^{-5} seconds^{-1} (Lloyd Instruments Ltd., West Sussex, UK). An extensometer was clipped to the specimen for correct estimation of elongation during the tension tests. The fractured surfaces of the specimens were also observed under the ZEISS EVO-50 scanning electron microscope (Carl Zeiss, Oberkochen, Germany) to analyze the nature of fracture of the SMA strips.

The shape-memory effect was characterized by carrying out a bend test on rectangular specimens with the dimensions 50 mm × 2 mm × 0.5 mm. This testing procedure allows for a first-order assessment of the shape-memory properties. A schematic diagram of the bend test arrangement is shown in Figure 2. The

specimens were bent to 180 deg by wrapping them around a cylindrical rod at ambient temperature. The specimen sprang back to an angle θ_1 after releasing at the same temperature. The specimen straightened after heating to a higher temperature, well above austenitic finish temperature (A_f), and came back to an angle θ_2. The shape recovery ratio (SRR) from a one-way SME was estimated using following expression: SRR = $[(\theta_1 - \theta_2)/\theta_1] \times 100$.

The two-way shape memory effect (TWSME) was induced in the rectangular SMA specimens by a training procedure consisting of bending them around the cylindrical rod followed by constrained heating–cooling cycles consisting of heating up to approximately 100 K above the A_f temperature and water quenching at room temperature. The specimens revert back to an angle θ_3 from θ_2 after water quenching because of TWSM effect (Figure 2). Several such training cycles were performed on the specimens to obtain the TWSM effect. The TWSM strain (ε_{tw}) was estimated using the expression: $\varepsilon_{tw} = [(\theta_3 - \theta_2)/180] \times \varepsilon_d$. The permanent plastic strain (ε_p) was estimated as follows: $\varepsilon_p = (\theta_2/180) \times \varepsilon_d$. The applied prestrain (ε_d) during bending was estimated from the specimen thickness (t) and the rod diameter (D); *i.e.*, $\varepsilon_d = [t/(t + D)] \times 100$. The applied prestrain can be adjusted by varying the diameter of the rod. In the current work, the shape-memory behavior of the Cu-Al-Ni strips was evaluated at 1, 2, and 4 pct applied prestrain.

III. RESULTS AND DISCUSSION

A. *Microstructural Characteristics of As-Mixed and Milled Powders Preforms*

Figure 3 shows typical SEM micrographs, using backscattered electron detector, of the green preforms prepared from mechanically mixed elemental powder mixture as well as from powder mixture milled for 2, 4, and 8 hours. It can be observed that the distribution of Cu, Al, and Ni in the preforms is clearly visible because of the color contrast. The Cu, Al, and Ni were identified from elemental distribution maps of the same area. Although the overall distribution of Cu and Al may seem to be uniform in the as-mixed powder compact (Figure 3(a)), it is extremely difficult to control the mixing in such a way that uniform distribution is achieved reproducibly. The segregation of Cu, Al, and Ni particles was found to occur during mixing because of particle size and density differences. Apart from the overall global distribution, fine local distribution of Cu, Al, and Ni is also an important aspect to ensure better chemical homogeneity during initial sintering as well as postrolling homogenization, which relies on the inter-diffusion of elements. From Figure 3(a), it can be observed clearly that the fine-size Cu and Al powder particles clustered together to form big regions of Cu and Al. Moreover, coarse Cu powder particles also formed concentrated regions of copper. It can also be observed that Ni powder particles are clustered and

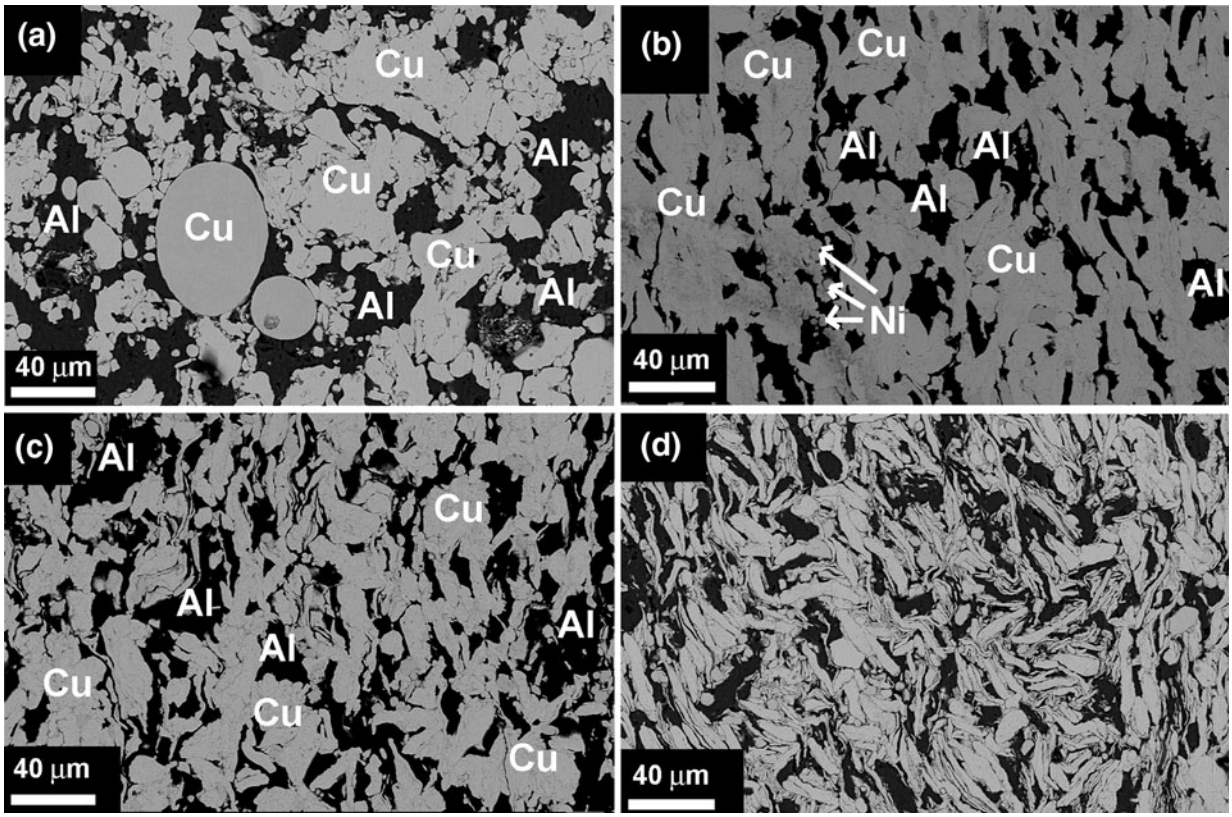

Fig. 3—Typical SEM micrographs, using backscattered electron detector, of the preforms prepared from (*a*) elemental powder mixture, and powder mixture milled for (*b*) 2 h, (*c*) 4 h, and (*d*) 8 h.

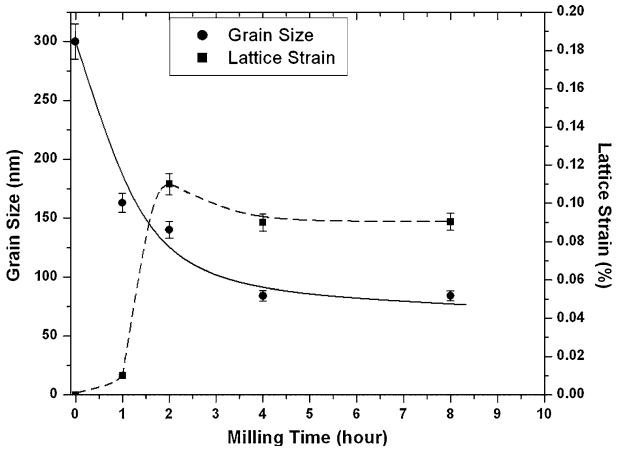

Fig. 4—Variation of lattice strain and grain size of the powder mixture with milling time.

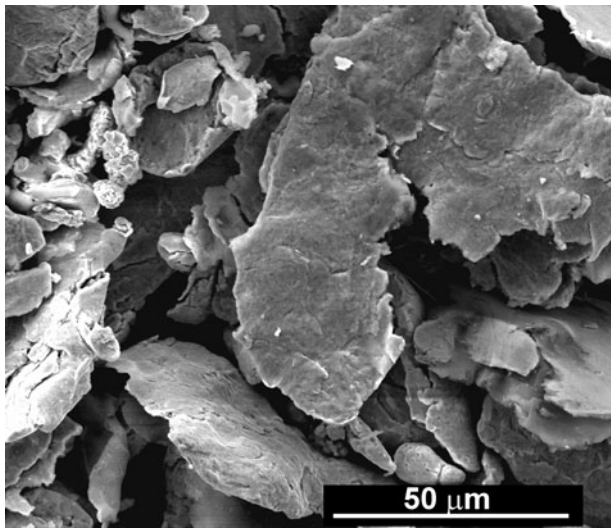

Fig. 5—Morphology of the powder particles milled for 8 h.

segregated in certain areas only. This scenario represents the situation wherein elemental distribution seems uniform globally but is nonuniform locally. Therefore, the mixture of elemental Cu, Al and Ni elemental powder, with a ratio of 82Cu-14Al-4Ni (wt pct), was ball milled in a high-energy ball mill for a short period of time to ensure uniform local distribution together with refined microstructure.

Two hours of milling (Figure 3(b)) resulted in more uniform distribution of Cu and Al, and the regions of Cu and Al reduced considerably in size. It can also be observed that powder particles have deformed and individual powder particles can barely be identified. Subsequent ball milling of the powder mixture for 4 hours resulted in a more uniform elemental distribution with a much finer microstructure, compared with 2-hours milled powder (Figure 3(c)). It can also be observed that a fine layered microstructure, consisting of Cu and Al layers, started to appear at this stage of milling. This stage of milling can be considered as the beginning of formation of regions with uniform local elemental distributions. It is interesting to note that the ball milling time of 8 hours resulted in very fine layered microstructure consisting of Cu and Al layers (Figure 3(d)). This stage can be considered an optimum condition, under the current milling conditions, which resulted in a satisfactory level of uniform local elemental distribution in the powder compact, as shown later.

Figure 4 shows the variation of lattice strain and grain size of the milled powder with increasing milling time. The grain size and lattice strain of the as-mixed as well as ball-milled elemental powder mixture were evaluated by XRD line broadening technique. In the current work, a single-line profile analysis procedure based on Voigt function representation was applied for the correct estimation of grain size and lattice strain.[30] It can be observed that the grain size decreased and lattice strain increased considerably after 8 hours of milling. It is well established that powder particles undergo severe plastic deformation during milling, which results in the accumulation of large amounts of dislocations and other defects. The accumulation of these defects is considered the key factor for grain refining and increased lattice strain. Therefore, the previous results indicate that high-energy ball milling of Cu, Al, and Ni elemental powder mixture for 8 hours led to the severe plastic deformation of powder particles, and milled powder particles consisted of large amounts of accumulated dislocations and other defects. Figure 5 shows the morphology of the powder particles milled for 8 hours, wherein a presence of thin, flaky, and fractured particles can be observed. The morphology of the powders transformed from irregular (elemental powders) to a thin, flaky shape. Such a morphology of particles indicated a severe plastic deformation leading to the refining of a layered structure together with the fracturing of particles. It can be envisaged that the layered structure along with accumulated defects, caused by severe plastic deformation, would enhance the rate of interdiffusion of elements. It is important to mention that additional milling would result in a much finer layered structure with a more uniform local elemental distribution. However, prolonged milling would also lead to the formation of a higher amount of alumina, which would not only alter the chemistry of the alloy but also pose problems in pore closure during consolidation. Figure 6 shows the elemental distribution of Cu, Al, Ni, and Oxygen in the 8-hour milled powder preforms. It can be observed that all the elements are distributed more or less uniformly in the matrix globally as well as locally. Therefore, elemental powder mixture milled for 8 hours was taken for subsequent processing in the current work.

B. *Microstructural Characteristics of Sintered Cu-Al-Ni Powder Preforms*

The preforms prepared from powder milled for 8 hours were sintered under a hydrogen atmosphere at 823 K (550 °C) for 1 hour. The sintering temperature was chosen below 933 K (660 °C) to avoid any melting of Al. The sintered powder preforms had a density of approximately 75 pct of the fully dense Cu-Al-Ni alloy. Figure 7 shows the XRD patterns of the 8-hours milled

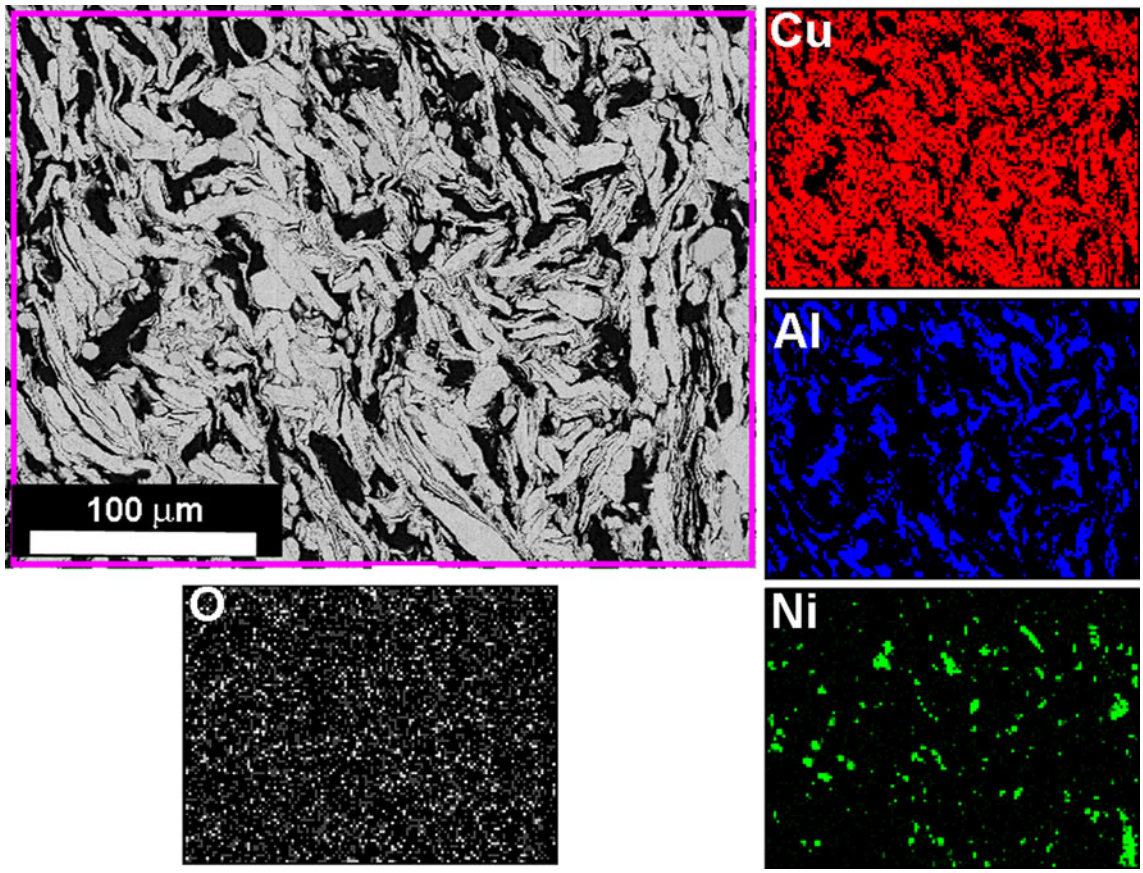

Fig. 6—Elemental distribution of Cu, Al, Ni, and oxygen in the preforms prepared from 8-hours milled elemental powder mixture.

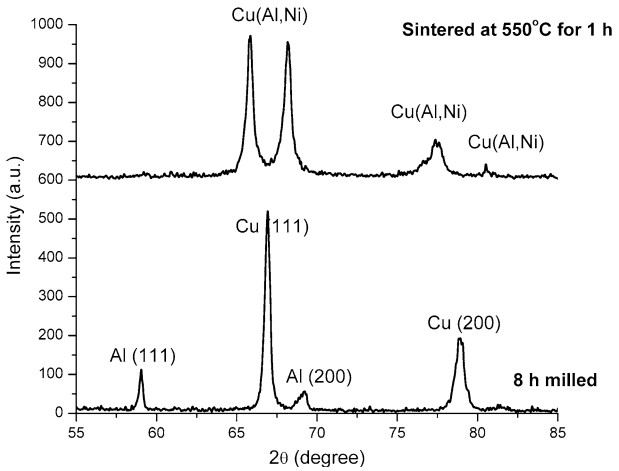

Fig. 7—XRD patterns of the 8-h milled elemental powder mixture and powder preforms sintered at 823 K (550 °C) for 60 min.

elemental powder mixture together with sintered preforms prepared from milled powders. It can be observed that the XRD pattern of milled powder consists of peaks corresponding to elemental Cu and Al. However, the peak of Ni is not visible because of its small amount in the mixture. Moreover, the presence of peaks corresponding to Cu and Al also indicates that no significant mechanical alloying occurred because of short-time high-energy ball milling of powder mixture. From Figure 7, it also can be observed clearly that the peaks corresponding to Cu and Al disappeared after sintering and new peaks appeared at different 2θ values than those of the elemental Cu and Al. Furthermore, it is interesting to note that two new peaks emerged in place of every Cu peak and their position was close to the original Cu peak. These changes in XRD spectra indicate the formation of two different Cu-rich solid solutions of Cu(Al, Ni) with different Al and Ni contents, as a result of sintering. Figure 8 shows a typical SEM micrograph, using a backscattered electron (BSE) detector, of the sintered Cu-Al-Ni powder compact. The color contrast in the BSE mode SEM micrograph depicts different phases with different compositions. An EDS analysis was carried out on different apparent phases (marked as 1, 2, and 3) to find out their composition, and the results are shown in Table I.

It can be noted that the areas marked as "1" are Ni-rich regions, whereas areas "2" and "3" are Cu-rich regions. These results indicate that sintering has mostly resulted in the formation of Cu-rich Cu-Al-Ni solid solutions. Additionally, a small amount of Ni-rich Cu-Al-Ni solid solution also formed during sintering. It would be important to mention that there was no evidence of the presence of either elemental Al or Al-rich solid solution in the sintered preform. It implies that Al fully dissolved during sintering and formed primarily Cu-rich solid solution along with a small amount of Ni-rich, Cu-Al-Ni solid solution. The implication of

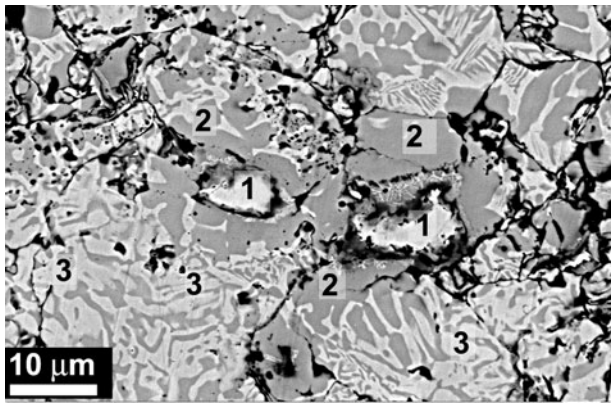

Fig. 8—A typical SEM micrograph, using BSE detector, of powder preforms sintered at 823 K (550 °C) for 60 min. The areas marked as "1" depict the regions of Ni-rich Cu-Al-Ni solid solution, and areas marked as "2" and "3" depict the regions of Cu-rich, Cu-Al-Ni solid solutions.

Table I. Chemical Composition of Different Phases in Sintered Cu-Al-Ni Preforms

	Average Composition (wt pct)		
Region	Cu	Al	Ni
1	12.1	24.47	60.43
2	76.3	17.18	6.52
3	88.82	9.95	1.23

these results is that the sintered preforms can be densified via hot-densification rolling at higher temperatures without the occurrence of any melting of aluminum.

C. *Hot Rolling of Sintered Powder Preforms*

The sintered Cu-Al-Ni alloy preforms were hot rolled at 1273 K (1000 °C) and approximately an 85 pct thickness reduction was achieved in three rolling passes. Sintered powders behaved well during hot rolling. Figure 9 shows the relationship between percent thickness deformation and percent length increase in the Cu-Al-Ni alloy strip during hot rolling at 1273 K (1000 °C). It can be observed that the rate of the length increment was small up to 25 pct thickness deformation, which suggests that most of the deformation produced during hot rolling is in the thickness direction, and a relatively small increase exists in the length of the strip. Furthermore, the rate of the length increment was moderate between 25 to 50 pct thickness deformations, whereas a rapid linear length increment was observed beyond 50 pct thickness deformations. Figure 10 shows the relationship between the relative density and fractional thickness deformation in Cu-Al-Ni strip during hot rolling at 1273 K (1000 °C). It can be observed that the density increased rapidly during the initial 25 pct thickness deformation. Beyond 25 pct thickness deformation, the relative density increased continuously, and near-full density is achieved after approximately 85 pct thickness deformation.

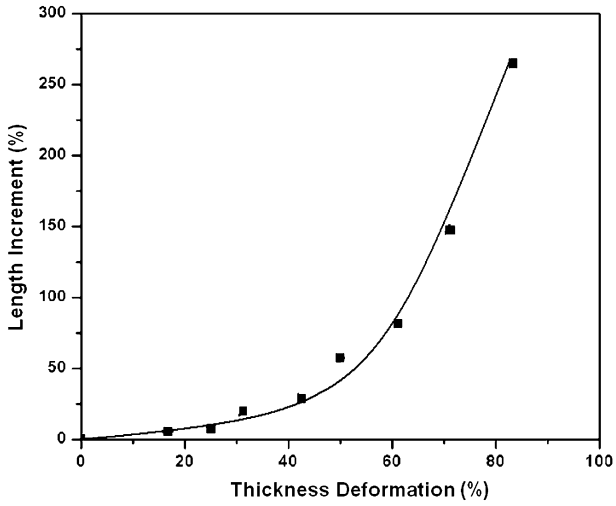

Fig. 9—Relationship between percent thickness deformation and percent length increase in sintered powder preforms during hot rolling at 1273 K (1000 °C).

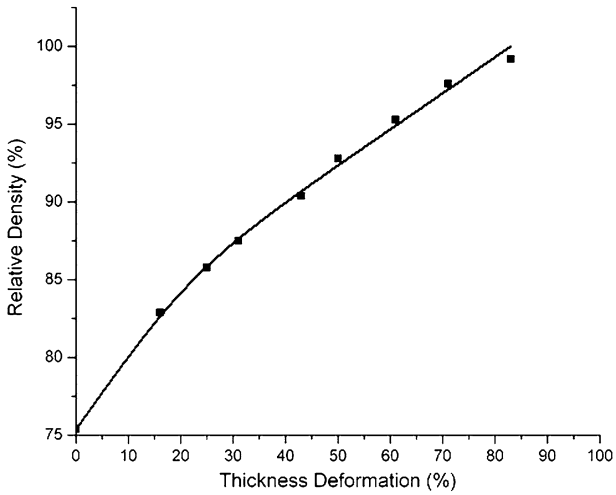

Fig. 10—Relationship between relative density and fractional thickness deformation in the sintered porous powder preforms during hot rolling at 1273 K (1000 °C).

Figure 11 shows a photograph of the hot-rolled Cu-Al-Ni strips. It can be observed that only minor edge cracks were present on the hot-rolled strips and no severe cracking occurred during hot rolling at 1273 K (1000 °C). Figure 12 shows a typical SEM micrograph of hot-rolled Cu-Al-Ni strip at its thickness cross-section parallel to the rolling direction. It is apparent that nearly full density was achieved in the finished strip by hot-densification rolling. Subsequently, the hot-rolled Cu-Al-Ni strips were homogenized at 1223 K (950 °C) for 6 hours under argon atmosphere.

D. *Microstructural Characteristics of Hot-Rolled and Homogenized Cu-Al-Ni Alloy Strips*

Figure 13 shows the XRD pattern of the hot-rolled Cu-Al-Ni alloy strip, which was homogenized for 6 hours at 1223 K (950 °C) followed by water quenching. The XRD

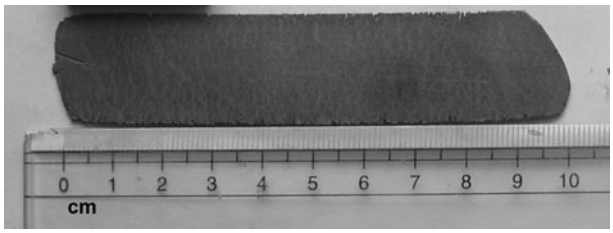

Fig. 11—A photograph of the hot-rolled Cu-Al-Ni strips.

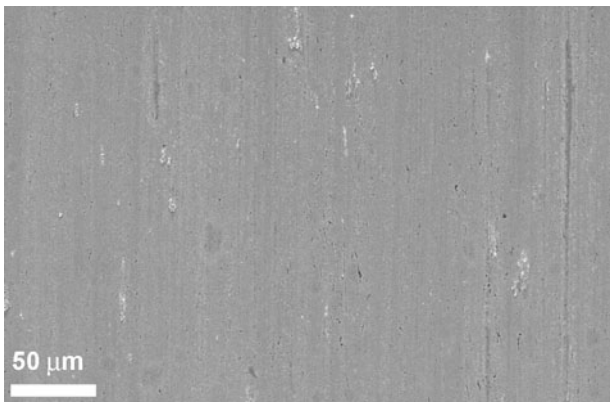

Fig. 12—A typical SEM micrograph of the hot-rolled Cu-Al-Ni strip on its thickness cross section parallel to rolling direction.

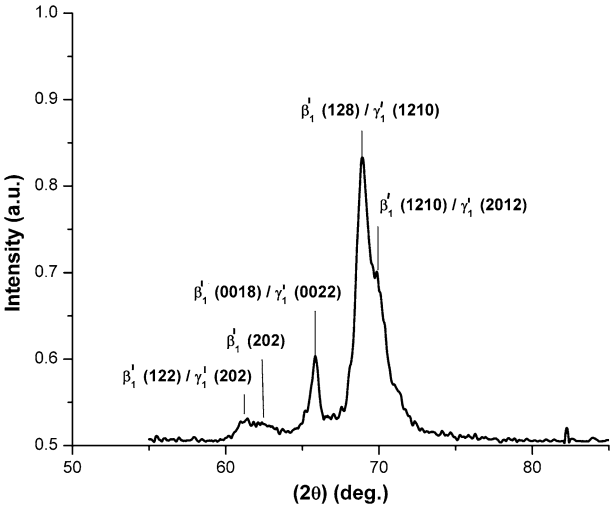

Fig. 13—XRD pattern of the hot-rolled Cu-Al-Ni alloy strip, homogenized for 6 h at 1223 K (950 °C), followed by water quenching.

pattern indicates that homogenized strips are almost fully martensitic in nature, consisting of a mixture of β_1' (monoclinic) and γ_1' martensites. However, the presence of some amount of retained austenite phase cannot be ruled out. Figure 14 shows SEM micrographs of homogenized Cu-Al-Ni strips. It can be observed that the homogenized strips were almost full of martensitic phase with two distinct types of morphologies, *i.e.*, irregular zigzag and parallel plate types. The irregular zigzag type of morphology is associated with β_1' martensite, whereas parallel

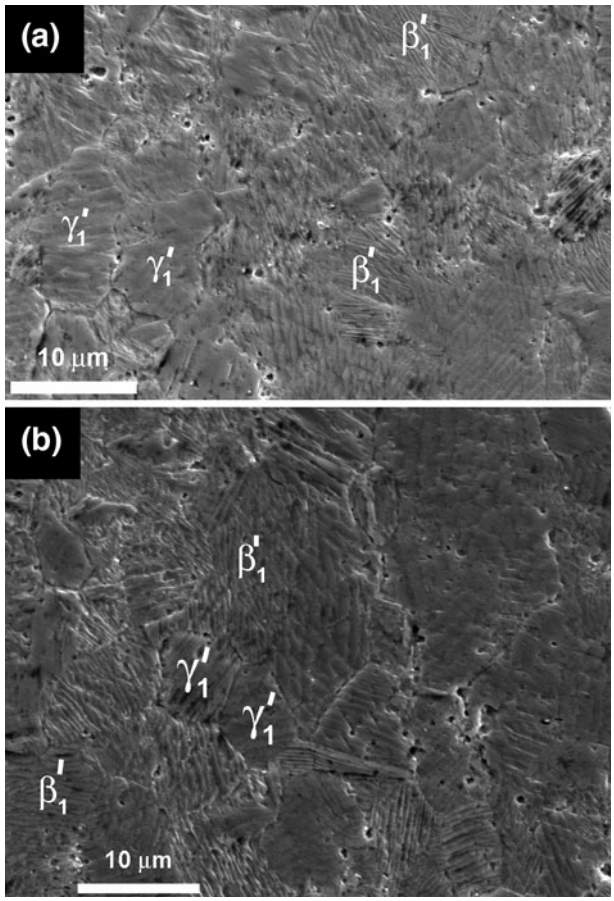

Fig. 14—Typical SEM micrographs of homogenized Cu-Al-Ni alloy strips showing the presence of fine-grained structure in almost fully martensitic state, consisting of both β_1' and γ_1' martensites.

plate type with γ_1' martensite.[31,32] Thus, the SEM micrographs confirm the stated results of the XRD analysis of the Cu-Al-Ni strips. The analysis also indicated that the finished strips were chemically homogeneous as no evidence was found regarding the presence of significant amount of either Al-rich or Ni-rich intermetallics.

Figure 15 shows a typical bright-field TEM micrograph of finished, *i.e.*, homogenized and water quenched, Cu-Al-Ni SMA strips, wherein the presence of self-accommodating variants of martensite can be observed clearly. Moreover, it can also be observed that the martensite plates consist of fine internal striations. Figure 16 shows dark-field TEM micrographs of finished Cu-Al-Ni SMA strips. The presence of parallel sided martensitic plates having fine internal striations can be clearly observed in Figure 16(a). Furthermore, Figure 16(b) shows a high-magnification TEM micrograph of the martensitic plate with fine internal striations, wherein the presence of stacking faults can be observed clearly. Swann and Warlimont[31] demonstrated that the fine internal striations inside martensitic plates appear because of the presence of a high density of stacking faults.[31] Moreover, the presence of antiphase domains boundaries of the superlattice structure, indicated by arrows, is also visible in the Figure 16(b).

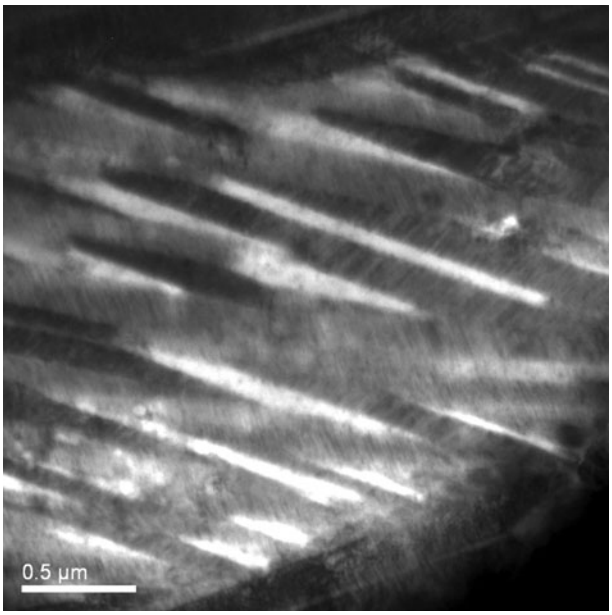

Fig. 15—A typical bright-field TEM micrograph of the homogenized Cu-Al-Ni strips, showing the presence of self-accommodated variants of martensite.

Figure 17 shows a typical TEM micrograph depicting the interface region of adjoining martensite plates, which consisted of a high density of stacking faults. It can be observed that the stacking faults are extended across the martensite plates. The presence of high-density stacking faults extending across martensite plates is a typical characteristic of β_1' martensite.[31]

From Figure 14(a), it can also be observed that the homogenized Cu-Al-Ni SMA strips had a fine-grained structure. The average grain size of the homogenized SMA strips was estimated from SEM micrographs by the linear intercept method, and it was found to be approximately 6 μm. It is interesting to note that the grain size of the Cu-Al-Ni SMA strips, prepared in the current work, is the smallest thermally stable grain size achieved in Cu-Al-Ni SMAs prepared by different processing routes.[12,15,20–23,28] Therefore, the current processing route provides an opportunity to prepare extremely fine-grained Cu-Al-Ni SMAs. The existence of such a fine-grained, thermally stable structure in the current homogenized Cu-Al-Ni SMA strips suggests the presence of some grain growth inhibitors on the grain boundaries. As a result, the grain boundary movement was restricted severely during the homogenization of the hot-rolled Cu-Al-Ni strips. To study the nature of the second-phase particles in the finished Cu-Al-Ni SMA strip, SEM and TEM studies were carried out, and these are discussed as follows.

The compositions of the matrix and the grain boundaries were evaluated by carrying out an EDS analysis under SEM. The composition of the matrix was estimated by point analysis at the center of the grains, whereas the composition of the grain boundaries was estimated by a point analysis on the grain boundaries. Several such analyses were carried out and the average composition was calculated (Table II).

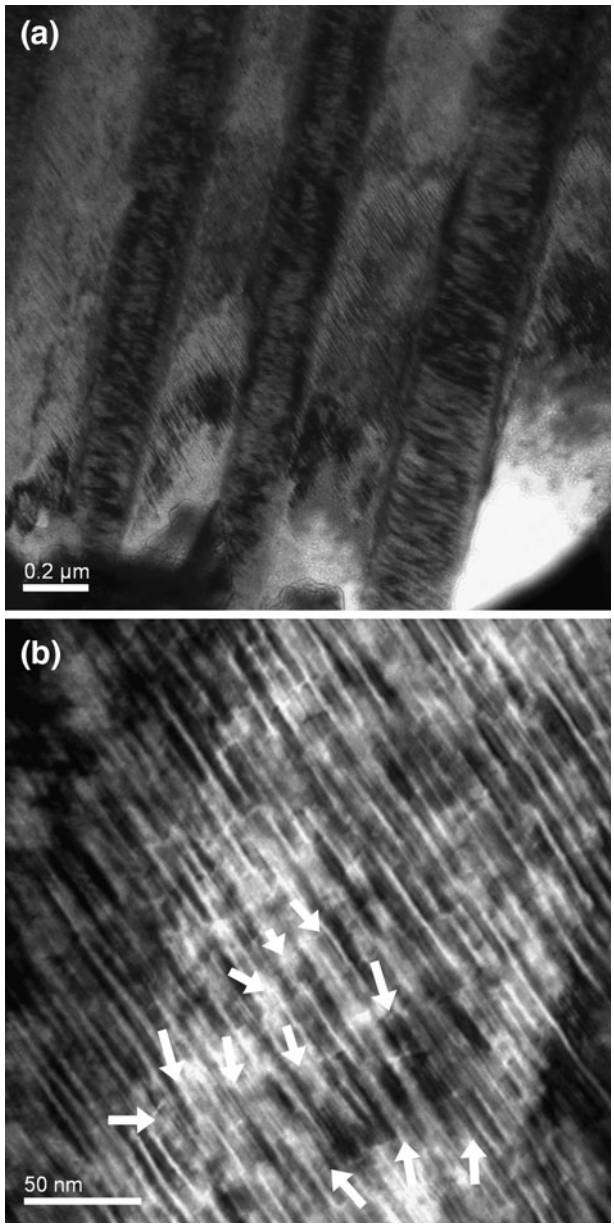

Fig. 16—Typical dark-field TEM micrographs of the finished Cu-Al-Ni SMA strips.

It can be noted that the Al content at the grain boundary region is relatively higher compared with the matrix. It can also be noticed that no appreciable amount of oxygen was detected in the matrix, whereas the grain boundary region was found to consist of substantial amounts of oxygen. The relatively higher amounts of aluminum, compared with the matrix, together with substantial amounts of oxygen in the grain boundary region indicate the possibility of the presence of alumina particles on the grain boundaries. Although the presence of any appreciable amount of oxygen inside the matrix was not detected by an EDS analysis in the SEM, the possibility of the presence of small amounts of alumina particles inside the matrix cannot be ruled out considering the limitations of the EDS analysis under SEM. As shown subsequently, this aspect has been confirmed by the TEM study.

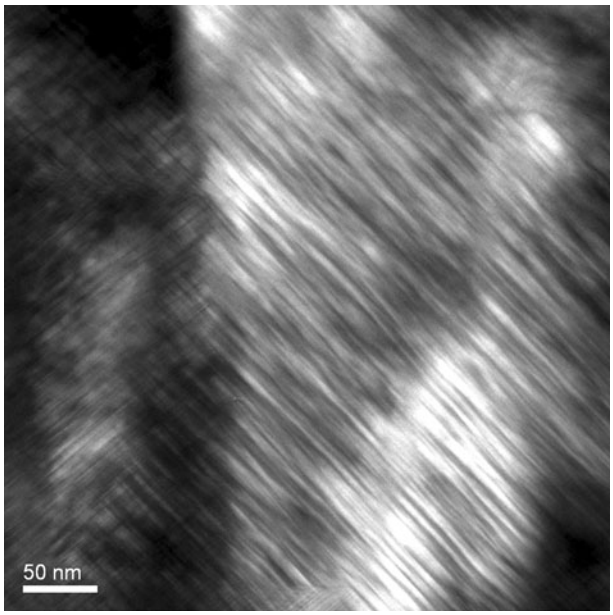

Fig. 17—A typical TEM micrograph showing the presence of stacking faults extended across the martensite plates.

Table II. Average Composition of the Matrix and Grain Boundaries

	Average Composition (wt pct)			
Region	Cu	Al	Ni	O
Matrix	83.39	12.07	4.54	Nil
Grain boundary	77.06	15.25	3.93	3.76

TEM studies were also carried out to understand the nature and distribution of second-phase particles present in the homogenized Cu-Al-Ni SMA strips. Figure 18 shows typical bright-field TEM micrographs of homogenized Cu-Al-Ni strips depicting the presence of nanosized particles on the grain boundaries as well as inside the matrix. It can be observed that nanosized particles, with a size in the range of 100 to 200 nm, were present on the grain boundary in the form of clusters (approximately 1 μm size) as well as individual particles (Figures 18(a) and (b)). Moreover, it can be observed also that the nanosized particles, with a size in the range of 100 to 200 nm, are also present inside the matrix (Figures 18(c) and (d)). It can be observed also that these particles are present not only as individual particles but also as clusters, similar to the particles that exist on the grain boundary. To identify these nanosized particles, the chemical composition of these particles was estimated using EDS in TEM by carrying out a point analysis in the scanning TEM mode. Table III shows the typical chemical composition of the particles that exist inside the matrix and on the grain boundary.

It can be noted that the particles had high aluminum and oxygen contents. Therefore, these particles can be identified as alumina (Al_2O_3) particles on the basis of the relative amounts of aluminum and oxygen content. However, it must be emphasized that most of the alumina particles were present on the grain boundaries, and only a small number of particles was present inside the matrix. No evidence was found regarding the presence of any other type of second-phase particles in the homogenized strips.

Alumina particles would have been introduced in the material the following two ways: (1) some amount of alumina particles already present on the surface of the argon-atomized aluminum powder particles and (2) formation of alumina particles during high-energy ball milling. It has been shown already that the high-energy ball milling of elemental Cu, Al, and Ni powder mixture for 8 h results in the plastic deformation of elemental powders leading to the formation of composite powder particles, consisting of fine alternate layers of Cu and Al. The alumina present on the starting aluminum powder would appear on the Cu/Al interface. During subsequent sintering, the layered structure present in the milled Cu/Al/Ni composite powder particle disappears, and each particle after sintering consists of Cu (Al, Ni) solid-solution matrix containing alumina, which was originally present on the Cu/Al interface. It can be envisaged that the distribution of alumina particles would become more uniform in the matrix during hot rolling of the sintered preforms. It seems that these alumina particles restrict the growth of the recrystallized grains during solutionizing/homogenization of the hot-rolled strips, leading to the formation of a fine-grained, thermally stable microstructure in the Cu-Al-Ni SMA strips.

E. *Mechanical Properties*

Figure 19 shows a typical stress–strain diagram of the hot-rolled and homogenized Cu-Al-Ni SMA strips. The average fracture stress and fracture strain values were approximately 677 MPa and 13 pct, respectively. Table IV shows a comparison of the mechanical properties of the Cu-Al-Ni SMA strips prepared via hot-densification rolling of sintered powder preforms prepared from different types of starting powders.

It can be noted that the average fracture stress and fracture strain of the current Cu-Al-Ni SMA strips are considerably higher than that of the Cu-Al-Ni SMA strips prepared from a mechanically blended powder mixture. Furthermore, it can also be noted that the average fracture stress and fracture strain of the current Cu-Al-Ni SMA strips are comparable with that of the Cu-Al-Ni SMA strips prepared from argon-atomized, prealloyed Cu-Al-Ni powder. Moreover, it is interesting to note that the average fracture strain of the current fine-grained Cu-Al-Ni SMA strips is one of the highest values obtained for polycrystalline Cu-Al-Ni alloys prepared by different processing routes.[11,17,18,24–29,33,34] Figure 20 shows typical SEM micrographs of the fractured surfaces of the tension test specimens. It is apparent that the mode of fracture is mixed type. It can be observed that the mode of fracture is a primarily void coalescence type in nature. However, a significant amount of transgranular mode of fracture can be observed also.

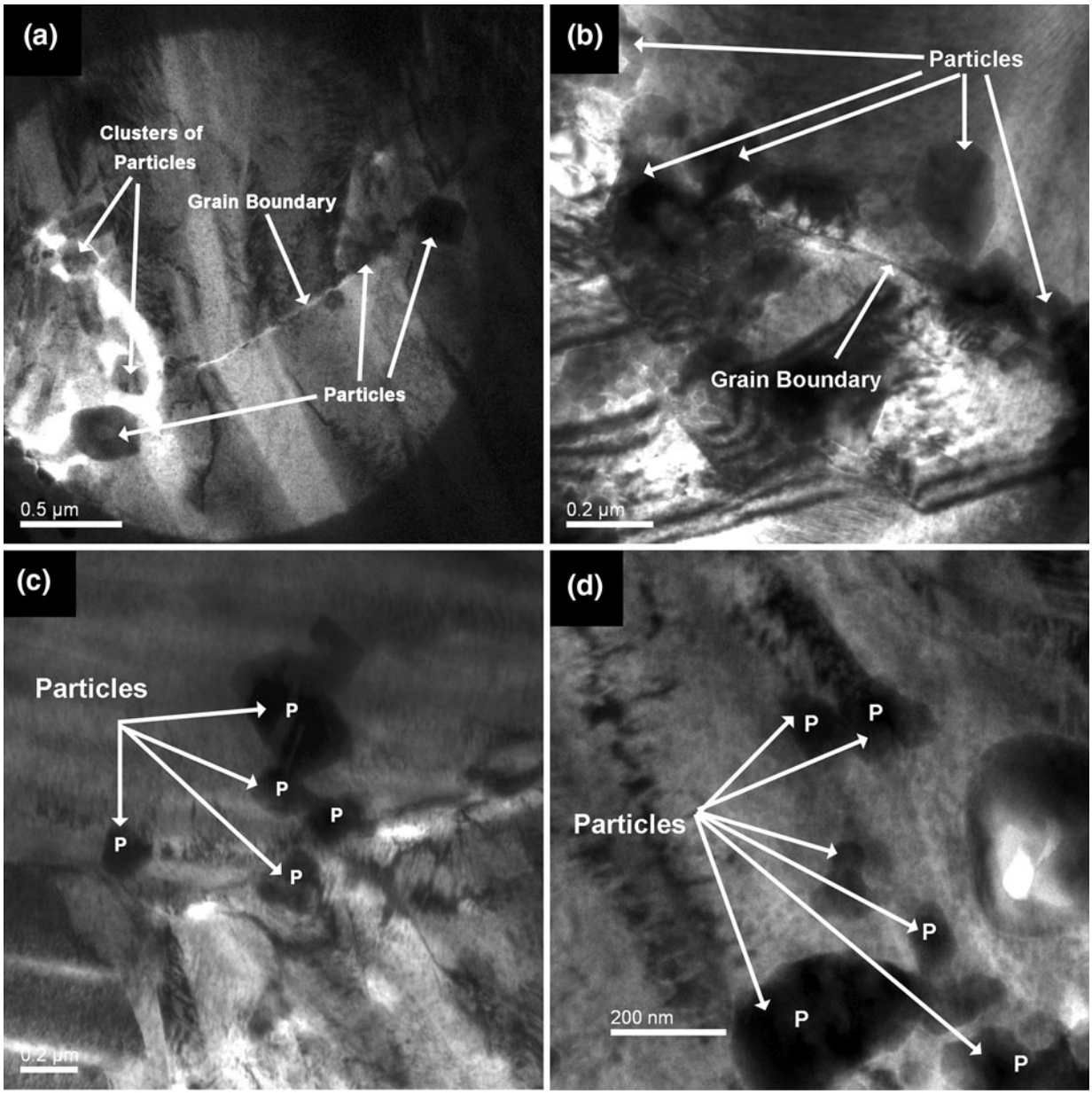

Fig. 18—Typical bright-field TEM micrographs showing the presence of nanosized particles (*a* and *b*) on the grain boundaries and (*c* and *d*) inside the matrix in finished Cu-Al-Ni SMA strips.

Table III. Typical Chemical Composition of the Particles Present on the Grain Boundary and Inside the Matrix of the Finished Cu-Al-Ni SMA Strips

	Average Composition (at pct)			
Region	Cu	Al	Ni	O
Nanosized particles present on the grain boundary	1.242	37.912	0.099	60.745
Nanosized particles present inside the matrix	2.371	36.235	0.210	61.182

At room temperature, the mode of fracture in the Cu-Al-Ni SMAs depends on the several factors, such as grain size, austenitic/martensitic state of specimen, and presence of second-phase particles. Sure and Brown[12] showed that the grain size has a significant effect on the mode of fracture in Cu-Al-Ni SMAs. The coarse-grained, single-phase austenitic Cu-Al-Ni SMA specimens, with a grain size greater than 100 μm, exhibited primarily intergranular type fracture, together with small areas of transgranular type. In contrast, fine-grained Cu-Al-Ni specimens, with a grain size less than 100 μm, show a primarily transgranular mode of fracture. In fine-grained

specimens, the grain boundary orientation changes over small distances and the crack propagation path encounters a large number of deviations. Consequently, the crack propagation path changes from an intergranular path to favorably oriented transgranular path, leading to a transgranular mode of fracture. The mode of fracture was also found to be dependent on the austenitic/martensitic state of single-phase Cu-Al-Ni SMA alloys. Miyazaki *et al.*[9] showed that the deformation of coarse-grained Cu-Al-Ni SMA specimens in the austenitic state resulted in the intergranular mode of fracture, whereas specimens in their martensitic conditions exhibited mostly transgranular mode of fracture together with some areas showing a dimpled ductile mode of fracture.

It has been demonstrated that a combination of fine grain size and martensite phase in the specimens leads to a microvoid-coalescence type mode of fracture in Cu-Al-Ni SMAs.[24,25,34] Mukunthan and Brown[34] showed that the fine-grained martensitic Cu-Al-Ni specimens, with a grain size of approximately 10 μm, exhibit an almost completely microvoid coalescence-type ductile nature of fracture. Recently, Vajpai *et al.*[24,25] also demonstrated that fine-grained Cu-Al-Ni SMA strips, with an average grain size of 27 to 90 μm, exhibit a primarily void-coalescence type mode of fracture when deformed in martensitic state. Furthermore, the presence of uniformly distributed, micron-sized, second-phase particles was also found to have a marked effect on the mode of fracture in the Cu-Al-Ni SMAs.[12] The fracture surface of fine-grained Cu-Al-Ni SMAs, with a grain size of 15 to 40 μm and consisting of uniformly distributed spherical second-phase particles of size 2 to 5 μm, exhibited a ductile microvoid coalescence-type mode of fracture.

The preceding discussion indicates that the fine-grained Cu-Al-Ni SMAs exhibit a transgranular mode of fracture when deformed in the austenitic state, whereas a microvoid coalescence type mode of fracture occurs when deformed in martensitic state and/or consist of microsized second-phase particles. It has been shown that the fine-grained Cu-Al-Ni SMA strips, which were prepared in the current work, are not only almost fully martensitic at room temperature but also consist of nanosized alumina particles on the grain boundaries as well as inside the matrix. Therefore, the microvoid

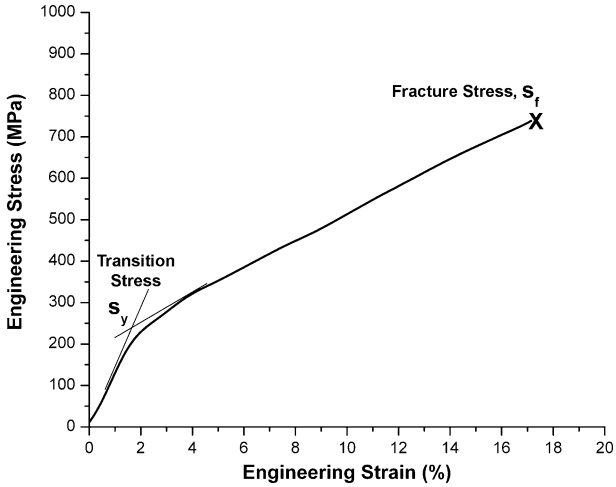

Fig. 19—A typical stress–strain diagram of finished Cu-Al-Ni SMA strips.

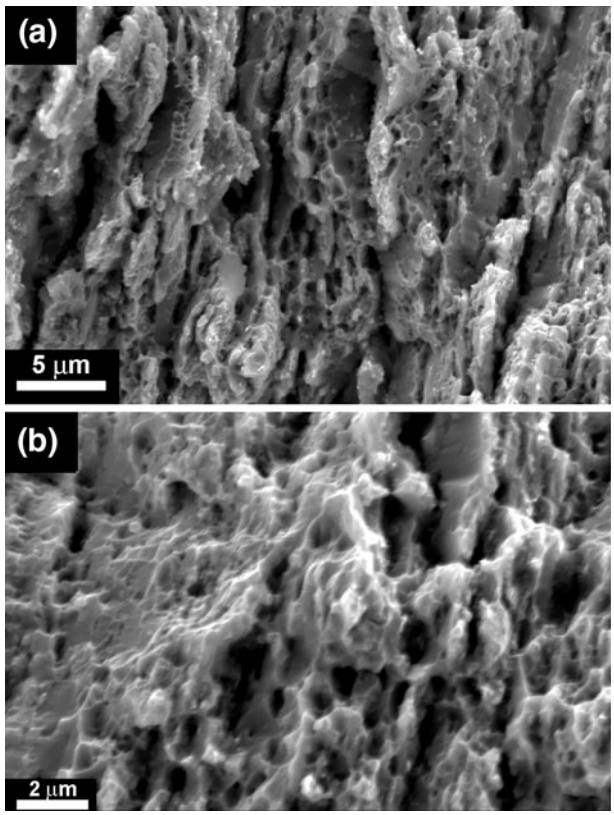

Fig. 20—Typical SEM micrographs showing the fractured surface of the tension test specimens prepared from finished Cu-Al-Ni SMA strips.

Table IV. Average Grain Size and Mechanical Properties of Cu-Al-Ni SMA Strips Prepared from Argon and Water Atomized Prealloyed Powders

Starting Powder Type	Grain Size of the Finished Cu-Al-Ni Strips (μm)	Fracture Stress (MPa)	Strain-to-Fracture (pct)	References
Argon atomized	90	530	12.6	24
Argon atomized	26	726	12.3	25
Mechanically blended powder mixture	10	470	5	28
Mechanically milled elemental powder mixture	6	677	13.1	Current work

coalescence type mode of fracture in the current Cu-Al-Ni SMA strips seems to be a combined effect of martensitic phase and nanosized alumina particles inside the matrix, together with small grain size. It seems that the presence of martensite phase and/or second-phase particles in fine-grained Cu-Al-Ni SMAs resulted in highly localized plastic deformation, leading to a microvoid coalescence type mode of fracture. Although it is difficult to separate the individual contribution of nanosized alumina particles and martensite phase on the mode of fracture at this stage, it is worth mentioning that most of the nanosized alumina particles were present on the grain boundaries, and only a small amount of particles was found to be present inside the matrix. Therefore, the microvoid coalescence type fracture in the current case can be attributed predominantly to the presence of martensite phase in the finished strips. Furthermore, the existence of some of the grains with retained austenite phase in the current Cu-Al-Ni SMA strips cannot be ruled out, considering the possibility of small local compositional variation inherent to the current powder metallurgy processing route involving elemental Cu, Al, and Ni powders. It seems that the presence of austenitic grains leads to the transgranular mode of fracture, as observed in Figure 20.

F. *Shape-Memory Properties*

Martensitic transformation is a first-order transformation wherein $\beta \Rightarrow$ martensite and martensite $\Rightarrow \beta$ transformations are exothermic and endothermic in nature, respectively. Figure 21 shows a typical thermogram of a specimen of the heat-treated Cu-Al-Ni strips in unstressed condition depicting the exothermic and endothermic peaks associated with $\beta \Rightarrow$ martensite and martensite $\Rightarrow \beta$ transformations, respectively. The characteristic transformation temperatures, *i.e.*, austenitic start (A_s), austenitic finish (A_f), martensitic start (M_s), and martensitic finish (M_f), are also indicated on Figure 21. It can be observed that the thermogram shows smooth transformation behavior during heating as well as cooling. The transformation hysteresis was estimated from peak positions, and it was found to be approximately 40 K (40 °C). The transformation hysteresis of 40 K (40 °C) is small considering the fine grain size of the specimens. A smooth transformation coupled with low hysteresis is a typical characteristic of $\beta_1 \Leftrightarrow \beta_1'$ transformation. Therefore, these results indicate that the heat-treated Cu-Al-Ni strips primarily form β_1' martensite on cooling, as shown previously.

Figure 22(a) shows the typical one-way shape recovery of Cu-Al-Ni SMA specimens with increasing temperature up to approximately full recovery. The Cu-Al-Ni SMA specimens were deformed in the martensitic state at room temperature applying 1, 2, and 4 pct deformation prestrain. It can be observed that shape recovery with increasing temperature was small initially, and thereafter, it increased rapidly and finally attained a saturation value. Because most of the shape recovery in a deformed

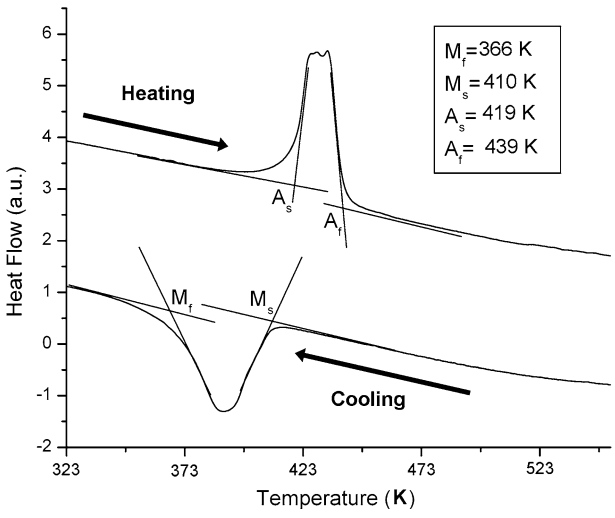

Fig. 21—A typical thermogram of the SMA specimens, in unstressed condition, prepared from the finished Cu-Al-Ni strips.

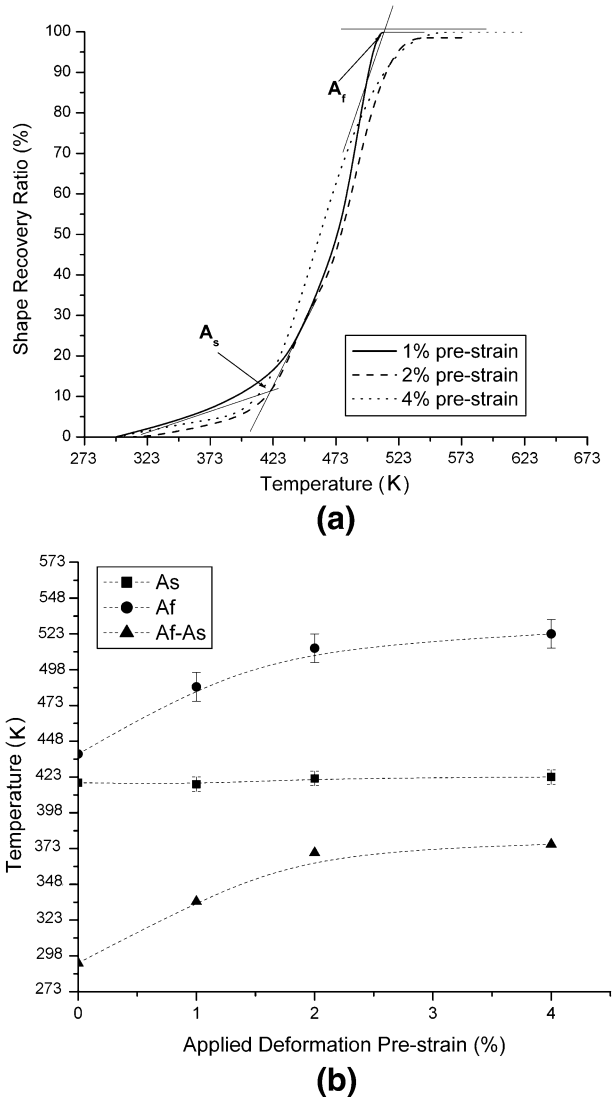

Fig. 22—(*a*) Typical one-way shape recovery of Cu-Al-Ni SMA specimens with increasing temperature and (*b*) variation of A_s, A_f, and $A_f - A_s$ with increasing deformation prestrain.

SMA is achieved between A_s and A_f, the temperatures corresponding to the beginning of rapid shape recovery and almost complete shape recovery were identified as A_s and A_f, respectively, as shown in Figure 22(a). Figure 22(b) shows the variation of A_s, A_f, and $A_f - A_s$ with increasing deformation prestrain. It is interesting to note that A_f increased continuously with increasing applied prestrain, whereas A_s remained more or less constant. Therefore, it seems that the A_s of the current fine-grained Cu-Al-Ni SMA remains unaffected by the extent of deformation prestrain, at least up to 4 pct applied deformation prestrain in the current case. Furthermore, it can also be observed (Figure 22(b)) that $A_f - A_s$ increases continuously with applied deformation prestrain. It is evident that the continuous increase in A_f is a consequence of increase in A_f with prestrain as the A_s remains more or less constant.

When SMAs are cooled below the M_f temperature, the formation of martensite in self-accommodating morphology results in the stored elastic energy and the stored elastic energy assists the reverse transformation.[35–37] It implies that the reverse transformation temperatures will be altered if this elastic energy is relaxed by predeformation of SMA in the martensitic state. For polycrystalline SMAs, it has been accepted that the stored elastic energy is relaxed not only by twin boundary movements but also by slip as a result of the movement of dislocations because of grain boundary constraints.[36,37] Such a relaxation in elastic stored energy seems to increase the driving force for reverse transformation, resulting in higher A_s and A_f. As a general trend, A_s and A_f have been found to increase with increasing deformation prestrain when SMA is deformed in its martensitic state.[36–39] However, the variation of the reverse transformation temperatures with the predeformation in polycrystalline SMAs depends on other factors such as the degree of deformation, mode of deformation, nature of martensite, etc.[36–40] Because polycrystalline specimens consist of several grains with different orientation, the state of stress would be different on each and every grain. This would result in structural heterogeneity in the deformed specimens even when deformed by uniaxial stress. If the specimen is deformed by bending, then the outer surface of the specimen will be deformed under tensile stress and the inner surface will be deformed by compressive stress. Such a mode of deformation will incorporate structural heterogeneity in the deformed specimens leading to the inhomogeneous distribution of dislocations. Therefore, the variation of reverse transformation with the degree of deformation in specimens deformed by bending might be different compared with the ones deformed by uniaxial stress. Hence, the continuous increase of A_f with increasing applied deformation prestrain in the current case seems to be the result of the stabilization of martensite after accumulated dislocations. In contrast, the small change in A_s might be related to the structural inhomogeneity in the deformed specimen resulting from nonuniform deformation.

Figures 23(a) through (c) show the shape of a specimen of martensitic Cu-Al-Ni SMA at room temperature in initial state, after bending at 4 pct applied prestrain, and recovered state. Interestingly, it seems that the specimen did not recover its initial shape completely even after heating to well above A_f (austenitic finish temperature). It would be worth mentioning that most of the residual "unrecovered" shape was caused by the appearance of two-way shape-memory effect even after first thermomechanical cycle consisting of bending, unconstrained heating to well above A_f, and cooling to room temperature. Figure 24 shows the evolution of two-way shape-memory strain with increasing number of training cycles at 4 pct applied prestrain. It can be observed that the two-way shape-memory strain increased rapidly up to approximately 10 training cycles, and a saturation level was

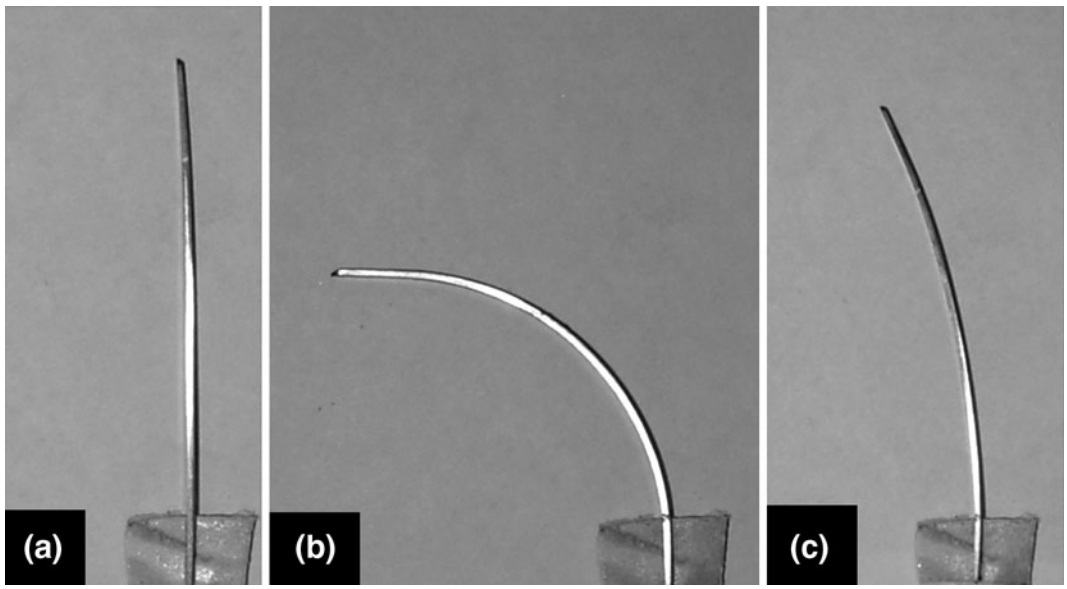

Fig. 23—Shape of the Cu-Al-Ni SMA strip: (*a*) initial, (*b*) deformed after 4 pct applied prestrain, and (*c*) recovered after heating to well above A_f followed by cooling to room temperature.

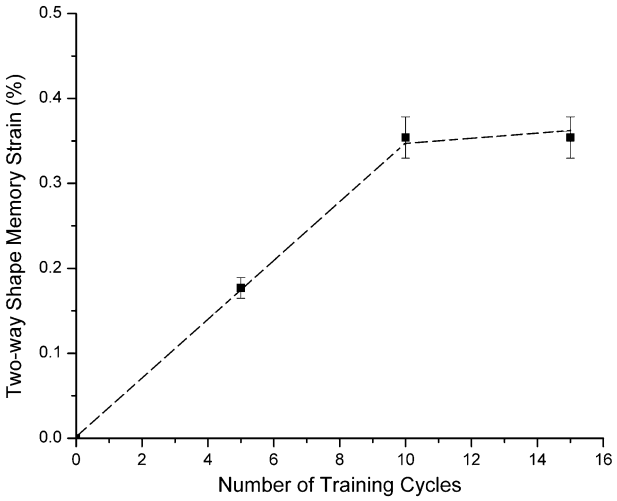

Fig. 24—The evolution of two-way shape-memory strain, at 4 pct applied training strain, with increasing number of training cycles.

achieved thereafter. A similar nature of two-way shape-memory strain evolution has also been observed in polycrystalline Ni-Ti, Cu-Zn-Al, Cu-Al-Ni, and monocrystalline Cu-Al-Ni alloys.[24,25,41–45] In the current work, the maximum value of two-way shape-memory strain was found approximately 0.35 pct after 15 training cycles at 4 pct applied training prestrain. Interestingly, the two-way shape-memory strain of the current Cu-Al-Ni strips is comparable with the Cu-Al-Ni SMAs prepared from argon-atomized powders and Ni-Ti–based SMAs under the similar training procedure and applied training strain.[24,25,43,44]

IV. CONCLUSIONS

Fine-grained Cu-Al-Ni SMA strips with an approximately 6- μm grain size, were prepared successfully from elemental powders via a powder metallurgy route involving high-energy ball milling of the starting powder mixture for a short time period, followed by powder preform preparation, sintering, and hot-densification rolling of the unsheathed sintered powder preforms. The high-energy ball milling of elemental powder mixture for 8 hours resulted in powder particles consisting of fine layers of Cu and Al. Cu, Al, and Ni were distributed more or less uniformly in the matrix globally as well as locally after 8 hours of ball milling. Sintering of powder preforms, at 823 K (550 °C) for 60 minutes, resulted in the formation of Cu-rich Cu-Al-Ni solid solution. The current study shows that the sintered powder preforms can be hot rolled successfully to near-full density under protective atmosphere at 1273 K (1000 °C), in unsheathed/uncanned condition. The densification in the sintered powder preforms was achieved primarily by hot rolling at 1273 K (1000 °C). A postconsolidation homogenization of hot-rolled strips at 1223 K (950 °C) for 6 hours resulted in the Cu-Al-Ni SMA strips having equiaxed grains of average size (approximately 6 μm). The homogenized Cu-Al-Ni SMA strips were almost fully martensitic in nature, consisting of a mixture of β_1' and γ_1' type martensites, and they exhibited an extremely good combination of strength and ductility. The average fracture stress and fracture strain of the strips were approximately 677 MPa and 13 pct, respectively. The fractured surfaces of the specimens exhibited primarily dimpled ductile nature of fracture, together with some transgranular type of fracture. The calorimetric studies exhibited smooth $\beta_1 \Leftrightarrow \beta_1'$ transformation behavior coupled with low transformation hysteresis ($\approx$ 40 K [40 °C]) and high characteristic transformation temperatures. An almost 100 pct one-way shape recovery was observed in specimens after bending followed by unconstrained heating at 1, 2, and 4 pct applied deformation prestrain. During two-way shape-memory training, the induced two-way shape-memory strain increased rapidly within the few initial training cycles, and a saturation level was attained after approximately 10 training cycles. The average maximum two-way shape-memory strain, induced after 15 training cycles, was found to be approximately 0.35 pct at 4 pct applied training strain.

ACKNOWLEDGMENT

The authors thank Dr. K. Mondal, Department of Materials and Metallurgical Engineering, Indian Institute of Technology, Kanpur, India, for providing the differential scanning calorimetry facility used in this investigation.

REFERENCES

1. P.K. Kumar and D.C. Lagoudas: *Shape Memory Alloys—Modeling and Engineering Applications*, D.C. Lagoudas, ed., Springer Science, New York, NY, 2008.
2. J.V. Humbeeck and S. Kustove: *Smart Mater. Str.*, 2005, vol. 14, pp. 5171–85.
3. J.V. Humbeeck: *J. Alloys Compd.*, 2003, vol. 355, pp. 58–64.
4. Z.C. Lin, W. Yu, R.H. Zee, and B.A. Chin: *Intermetallics*, 2000, vol. 8, pp. 605–11.
5. C.M. Wayman: *J. Met.*, 1990, pp. 129–37.
6. T. Tadaki: *Shape Memory Materials,* K. Otsuka and C.M. Wayman, eds., Cambridge University Press, Cambridge, UK, 1998.
7. J. Font, E. Cesari, J. Muntasell, and J. Pons: *Mater. Sci. Eng. A*, 2003, vol. 354, pp. 207–11.
8. L. Delaey: *Phase Transformation in Materials*, P. Haasen, ed., VCH, Weinheim, Germany, 1991.
9. S. Miyazaki, K. Otsuka, H. Sakamoto, and K. Shimizu: *Trans. Jpn. Inst. Met.*, 1981, vol. 22, pp. 244–52.
10. S.W. Husain and P.C. Clapp: *J. Mater. Sci.*, 1987, vol. 22, pp. 2351–56.
11. K. Sugimoto, K. Kamei, H. Matsumoto, S. Komatsu, K. Akamatsu, and T. Sugimoto: *J. Phys.*, 1982, vol. 43, pp. C4-761–66.
12. G.N. Sure and L.C. Brown: *Metall. Trans. A*, 1984, vol. 15A, pp. 1613–21.
13. J.S. Lee and C.M. Wayman: *Trans. Jpn. Inst. Met.*, 1986, vol. 27, pp. 584–91.
14. K. Adachi, K. Shoji, and Y. Hamada: *ISIJ Int.*, 1989, vol. 29, pp. 378–87.
15. J.W. Kim, D.W. Roh, E.S. Lee, and Y.G. Kim: *Metall. Trans. A*, 1990, vol. 21A, pp. 741–74.
16. D.W. Roh, J.W. Kim, T.J. Cho, and Y.G. Kim: *Mater. Sci. Eng. A*, 1991, vol. A136, pp. 12–23.
17. M.A. Morris: *Acta Metall. Mater.*, 1992, vol. 40, pp. 1573–86.

18. S. Bhattacharya, A. Bhuniya, and M.K. Banerjee: *Mater. Sci. Technol.*, 1993, vol. 9, pp. 654–58.
19. Y. Gao, M. Zhu, and J.K.L. Lai: *J. Mater. Sci.*, 1998, vol. 33, pp. 3579–84.
20. T.W. Duerig, J. Albert, and G.H. Gessinger: *J. Met.*, 1982, pp. 14–20.
21. R.D. Jean, T.Y. Wu, and S.S. Leu: *Scripta Metall. Mater.*, 1991, vol. 25, pp. 883–88.
22. S.S. Leu, Y. Chen, and R.D. Jean: *J. Mater. Sci.*, 1992, vol. 27, pp. 2792–98.
23. R.B. Parez-Saez, V. Recarte, M.L. No, O.A. Ruano, and J. San Juan: *Adv. Eng. Mater.*, 2000, vol. 2, pp. 49–53.
24. S.K. Vajpai, R.K. Dube, and S. Sangal: *Metall. Mater. Trans. A*, 2011, vol. 42A, pp. 3178–89.
25. S.K. Vajpai, R.K. Dube, and S. Sangal: *Mater. Sci. Eng. A*, 2011, vol. 529A, pp. 378–87.
26. S.M. Tang, C.Y. Chung, and W.G. Liu: *J. Mater. Process. Technol.*, 1997, vol. 63, pp. 307–12.
27. Z. Li, Z.Y. Pan, N. Tang, Y.B. Ziang, N. Liu, M. Fang, and M. Zheng: *Mater. Sci. Eng. A*, 2006, vol. 417, pp. 225–29.
28. M. Sharma, S.K. Vajpai, and R.K. Dube: *Metall. Mater. Trans. A*, 2010, vol. 41A, pp. 2905–13.
29. M. Sharma, S.K. Vajpai, and R.K. Dube: *Powder Metall.*, 2011, vol. 54, pp. 620–27.
30. S.K. Vajpai, R.K. Dube, and M. Sharma: *J. Mater. Sci.*, 2009, vol. 44, pp. 4334–41.
31. P.R. Swann and H. Warlimont: *Acta Metall.*, 1963, vol. 11, pp. 511–27.
32. V. Recarte, R.B. Perez-Saez, E.H. Bocanegra, M.L. No, and J. San Juan: *Metall. Mater. Trans. A*, 2002, vol. 33A, pp. 2581–91.
33. S. Miyazaki, T. Kawai, and K. Otsuka: *Scripta Metall.*, 1982, vol. 16, pp. 431–36.
34. K. Mukunthan and L.C. Brown: *Metall. Trans. A*, 1988, vol. 19A, pp. 2921–29.
35. L. Delaey, R.V. Krishnan, H. Tas, and H. Warlimont: *J. Mater. Sci.*, 1974, vol. 9, pp. 1521–35.
36. M. Piao, K. Otsuka, S. Miyazaki, and H. Horikawa: *Mater. Trans. JIM*, 1993, vol. 34, pp. 919–29.
37. K. Otsuka and X. Ren: *Progr Mater. Sci.*, 2005, vol. 50, pp. 511–678.
38. Y. Zheng, L. Cui, F. Zhang, and D. Yang: *J. Mater. Sci. Technol.*, 2000, vol. 16, pp. 611–14.
39. F. Chen, Y.X. Tong, B. Tian, L. Li, and Y.F. Zheng: *Mater. Lett.*, 2010, vol. 64, pp. 1879–82.
40. S.P. Belyaev, N.N. Resnina, and A.E. Volkov: *Mater. Sci. Eng. A*, 2006, vols. 438–40, pp. 627–29.
41. R. Lahoz, L. Gracia-Villa, and J.A. Puertolas: *J. Eng. Mater. Technol.*, 2002, vol. 124, pp. 397–401.
42. H.W. Kim: *J. Mater. Sci.*, 2005, vol. 40, pp. 211–12.
43. X.L. Meng, Y.F. Zheng, W. Cai, and L.C. Zhao: *J. Alloy Compd.*, 2004, vol. 372, pp. 180–86.
44. L. Wang, X. Meng, W. Cai, and L. Zhao: *J. Mater. Sci. Technol.*, 2001, vol. 17, pp. 13–14.
45. H. Sakamoto, K. Sugimoto, Y. Nakamura, A. Tanaka, and K. Shimizu: *Mater. Trans. JIM*, 1991, vol. 32, pp. 128–34.